Remote Sensing Letters

ISSN: (Print) (Online) Journal homepage: www.tandfonline.com/journals/trsl20

Monitoring a high mountain glacier through georeferenced time-lapse photography: Tapado, Dry Andes of Chile (30°S)

Sebastián Vivero

To cite this article: Sebastián Vivero (2024) Monitoring a high mountain glacier through georeferenced time-lapse photography: Tapado, Dry Andes of Chile (30°S), Remote Sensing Letters, 15:4, 443-455, DOI: 10.1080/2150704X.2024.2337609

To link to this article: https://doi.org/10.1080/2150704X.2024.2337609

Published online: 08 Apr 2024.

REMOTE SENSING LETTERS
2024, VOL. 15, NO. 4, 443–455
https://doi.org/10.1080/2150704X.2024.2337609

Taylor & Francis
Taylor & Francis Group

Monitoring a high mountain glacier through georeferenced time-lapse photography: Tapado, Dry Andes of Chile (30°S)

Sebastián Vivero [a,b]

[a]Department of Geosciences, University of Fribourg, Fribourg, Switzerland; [b]Drones for Earth (D4E), Lausanne, Switzerland

ABSTRACT

Glaciers and snow cover provide freshwater for irrigated agriculture and urban consumption in the Dry Andes. Given the aridity of this environment, sublimation losses are significant, making precise monitoring techniques crucial in estimating glacier changes. Continuous monitoring of glaciers is typically conducted through the use of automatic weather stations (AWS). However, these stations may not capture the full extent of glacier changes, warranting the use of additional monitoring techniques such as close-range remote sensing and satellite imagery. This study utilizes time-lapse photography acquired from 2013 to 2015 to examine the temporal and spatial albedo variations across the Tapado Glacier, along with the surface changes in the debris-covered section. Sequential orthorectified images were used to observe the spatial evolution of ice cliffs and supraglacial ponds as they changed over time. High-resolution displacement measurements were obtained using feature tracking methods on the debris-covered glacier. Additionally, distributed albedo maps were produced by comparing photographic data with point albedo measurements from an AWS. The results indicate decreased albedo values during summer, along with the expansion of supraglacial ponds and ice cliffs in the debris-covered region. The study also proposes a cost-effective remote site monitoring approach using time-lapse photography for continuous observation and data collection.

ARTICLE HISTORY
Received 9 November 2023
Accepted 23 March 2024

KEYWORDS
Glacier; albedo; time-lapse photography; dry Andes

1. Introduction

In the Dry Andes region (17°30´–35°S, 69°–70°W), glaciers and snow cover are essential elements of the hydrological cycle. The snowpack accumulated during winter is an important water source for major rivers and cities in this region (Favier et al. 2009), providing water for drinking, agriculture, and mining projects. Moreover, glaciers in the Dry Andes have also experienced widespread shrinkage, losing mass and area due to increased melting and reduced accumulation (Caro, Condom, and Rabatel 2021). Monitoring and understanding glaciers and snow cover in the Dry Andes is imperative due to their impact on water availability, ecosystem services, natural hazards and socio-economic development (Farías-Barahona et al. 2020).

CONTACT Sebastián Vivero sebastian.viveroandrade@unifr.ch Department of Geosciences, University of Fribourg, Ch. du Musée 4, Fribourg CH-1700, Switzerland

Glaciers and snow cover in the Dry Andes have been assessed spatially and temporally using remote sensing techniques, providing valuable information for glaciological and hydrological research (Farías-Barahona et al. 2020; Robson et al. 2022; Stehr and Aguayo 2017). However, more detailed field measurements and ground-based observations are needed to validate and complement the satellite data (Peña and Olmedo 2019), as well as to improve the modelling and projection of future scenarios of glacier and snow dynamics under climate change.

The use of terrestrial time-lapse photography has long been established as a simple and effective low-cost method of monitoring glacial and periglacial processes, including glacier velocity fields (Harrison et al. 1992; Maas et al. 2013), snow and ice albedo (Corripio 2004; Dumont et al. 2009). Instead of relying on stereo vision methods (two camera positions), single oblique images can be used in combination with digital elevation models to make the spatial georeferencing of these images (i.e., monoplotting) more approachable (Luhmann et al. 2014). Monoplotting techniques are frequently utilized to provide spatial information in images for further analysis, such as tracking snow lines (Barandun et al. 2018) and rock glacier displacement (Scapozza et al. 2014). However, this method of monitoring has not yet reached a sufficient level of use in the Andes as a result of it not being widely adopted.

The main aim of this research is to monitor spatial and temporal changes in a high-altitude glacier and a debris-covered glacier with a high degree of granularity. The main objectives are to: 1) document daily distributed albedo changes on a remote high-altitude glacier. 2) Detect persistent ice ponds and cliffs and measure the horizontal surface velocity through feature tracking on the lower debris-covered glacier. For this purpose, a camera was installed on the hillside south of the Tapado Glacier site to take daily image sequences.

2. Study area

The Cerro del Tapado is located at an elevation of 5,536 m a.s.l. (30° S, 69° W,). A semiarid climate dominates the region, influenced mainly by extratropical precipitation systems during the austral winter months (Garreaud 2007), although some convective activity does occur during the summer (Vuille and Keimig 2004). There is a complex glacio-geomorphologic assemblage associated with the Tapado Glacier comprised of rock glaciers, moraines, and debris-covered glaciers (Monnier et al. 2014; Vivero et al. 2021). Between 2013 and 2015, in-situ mass balance measurements proved very challenging conditions due to the high elevation range and irregular surface ablation patterns (DGA 2015). Furthermore, the area exhibits a great variety of glacial and periglacial processes, where permafrost occurrence is widespread (Azócar, Brenning, and Bodin 2017).

3. Methodology

3.1. Meteorological data

An automatic weather station (AWS) was installed in November 2013 on snow cover remaining from the winter period on the ablation zone of the Tapado Glacier (Figure 1). The AWS was equipped with a Campbell CR3000 datalogger programmed to acquire data every 10 minutes, averaging every hour. Station measurements include shortwave and longwave radiation (incident and reflected),

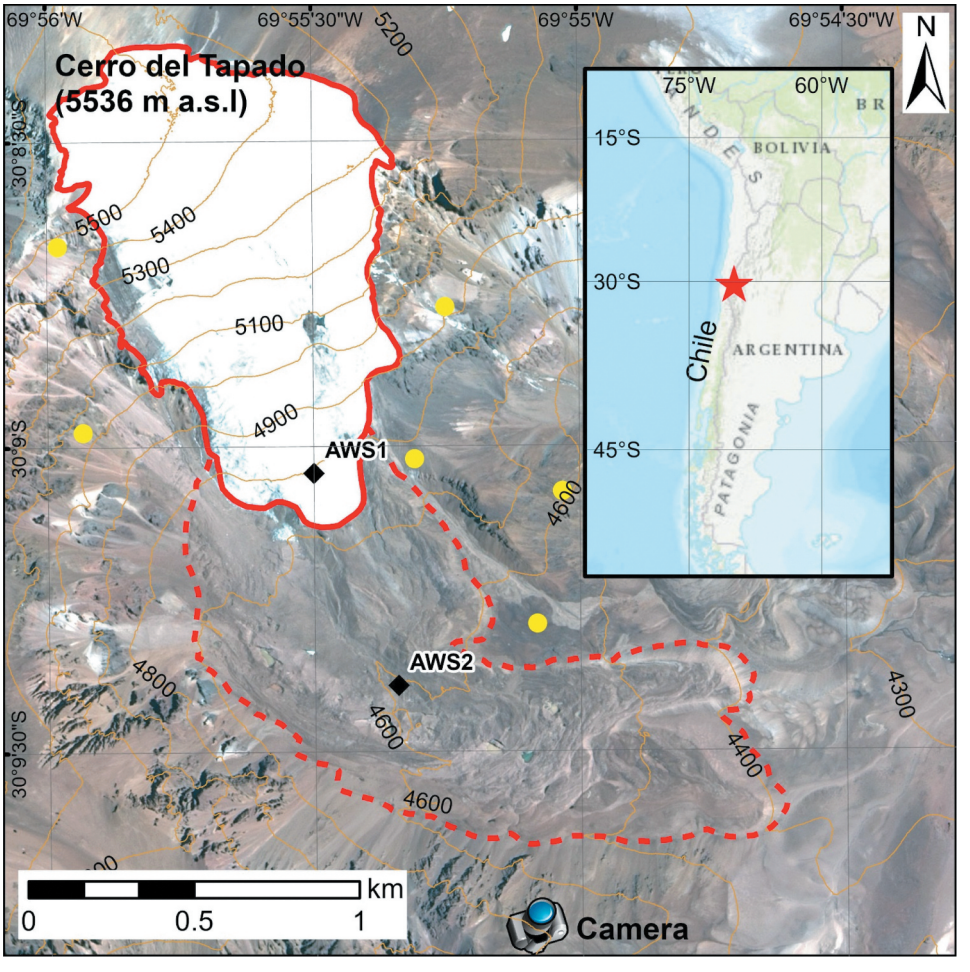

Figure 1. Inset: Location of the study area (red star), near the border between Argentina and Chile. Tapado Glacier (solid red line) and the glacier forefield, debris-covered glacier, push moraines, and rock glacier complex (dashed red line). The time-lapse camera is positioned on a mountain ridge at 4702 m a.s.l. Black rhombi indicate the position of the two AWS and yellow circles the position of the GCPs. Background imagery from © CNES (2018), and Airbus DS (2018), all rights reserved.

temperature and relative humidity (artificially aspirated), wind speed and direction, atmospheric pressure, and a sonic ranging sensor (snow/ice depth). The albedo of the AWS was calculated as the ratio of instantaneous measurements of incident and reflected shortwave radiation using a Kipp and Zonen CNR4 net radiometer. The AWS includes measurements of the tilt angle relative to the vertical. This tilt data exposes how quickly the station loses its vertical position, due to the generation of an irregular surface caused by the appearance and development of snow and ice penitentes. In addition to the AWS installed on the ablation zone, a secondary AWS with the same instruments was installed in late November 2013 in the Tapado debris-covered zone (Figure 1).

3.2. Camera setup

A Harbortronics autonomous time-lapse camera package was initiated on 21 November 2013, on a ridge located 1.5 km southeast of the central part of the Tapado Glacier. The sequential equipment consists of a CANON EOS digital Rebel XS camera (22.2 × 14.8 mm sensor dimensions), a Digisnap electronic trigger, a lithium battery, and a 12-volt solar panel. The camera was focused on the glacier with a focal length of 18 mm. Daily photographs were taken at 8:00 and 10:00 a.m., storing the images in the camera's native format (*.CR2). All 10:00 a.m. photographs were transformed to TIF format for further processing. These times were chosen because of the low probability cloud cover and precipitation due to the summer convective activity in this type of environment.

3.3. Orthoimages from oblique photographs

The transformation of digital photographs into orthoimages consists of establishing the geometric relationship between the internal and external orientation of the camera and the terrain. Oblique ground-based photographs are first corrected automatically for lens distortion using the PTLens software (https://www.epaperspress.com/ptlens/) with a general model specific for CANON cameras. It employs the commonly used polynomial model to describe radial distortion, with *a*, *b*, and *c* coefficients specific to each lens (Wang, Qiu, and Shao 2009). The result was the removal of the radial distortion normally present in these types of camera lenses. The digital photographs were then orthorectified using the method provided by Corripio (2004) to associate each pixel of the photograph with the correct position and elevation of the terrain.

The first part consists of georeferencing the oblique photographs, by applying a perspective projection of the photograph to a high-resolution DEM of the study area (Figure 2). For this, a Pléiades-derived DEM at 0.4 m resolution from 2014 Vivero et al (2021) was used. The series of images were processed using the Environment for Visualization (ENVI)-Interactive Data Language (IDL) software version 8.8 in a batch mode. Two differential GNSS (dGNSS) surveying campaigns were carried out in November 2013 and December 2014 to determine the position of the time-lapse camera as well the position of the respective AWS. In addition, the position of at least six GCPs was measured in order to help orient the camera and evaluate the orthorectification. This was done in an iterative manner until an optimal orientation was achieved. The final root-mean-square error (RMSE) was 0.08 m for both easting and northing coordinates.

3.4. Surface changes

The analysis of debris-covered glacier surface changes was achieved through the interpretation of high-resolution orthoimagery (i.e., photointerpretation), which helped in identifying supraglacial ponds, ice cliffs, and other features. The digitization of supraglacial ponds and ice cliffs was directly conducted in ArcGIS 10.8 by utilizing the high-resolution orthoimages obtained from the time-lapse camera. By multiplying the perimeter of the features with the spatial resolution, which is

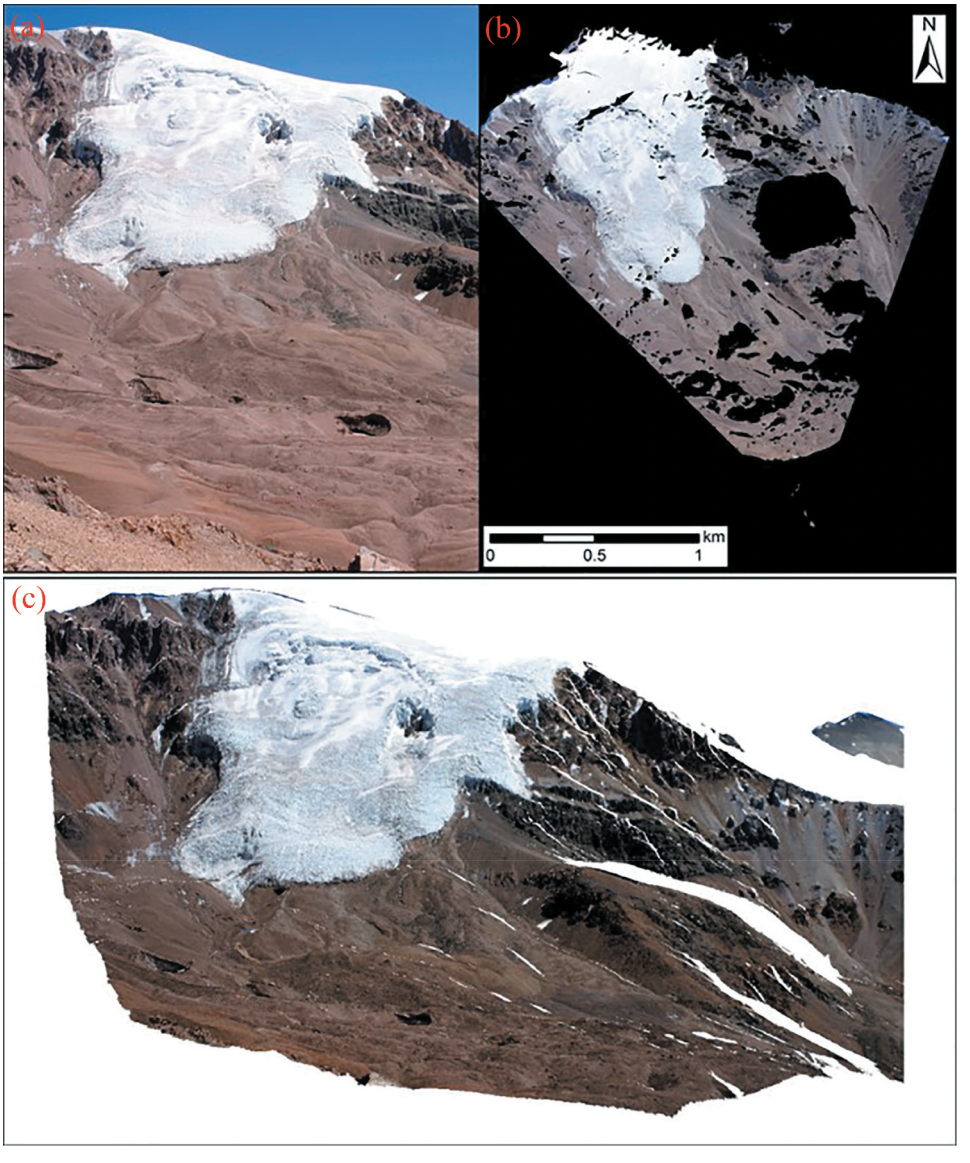

Figure 2. Transformation from digital photographs to orthoimages: (a) an original oblique photograph from the vantage point capturing Cerro del Tapado and its glaciers, (b) scaled orthoimage of the Tapado area using the high-resolution DEM, (c) 3D orthoimage visualization of Cerro del Tapado and its glaciers using the high-resolution DEM. Example using data acquired on January 5, 2014.

rounded to 0.5 m, the margin of error in determining the area was estimated for all identified features (Casassa, Rodríguez, and Loriaux 2014).

3.5. Feature tracking

Surface movements were assessed by automatically tracking features and manually tracing topographic features such as persistent boulders. To track surface movements,

CIAS software programmed in IDL was used, which employed the normalized cross-correlation operator (Kääb 2021). Reference and search window sizes were adjusted to the original spatial resolution of the repeated orthomosaics. Outlier detection was performed according to slope analysis and locally coherence displacement flow fields. Displacements were then converted into metres per year based on the time interval. Finally, the quality of feature tracking was evaluated by examining the relative accuracy, specifically the deviation of two data sets within unchanged areas outside the glacier.

3.6. Albedo maps

The albedo mapping consists of the transformation of the georeferenced image into albedo values, using meteorological data obtained from the AWS on the glacier and several metrics from the high-resolution DEM. Most of these metrics were estimated using the Raster Terrain Analysis Plugin in QGIS and SAGA libraries. The original methodology for calculating albedo from terrestrial photography was developed by Corripio (2004). Further improvements were made in Dumont et al. (2009). For detailed technical aspects of this methodology, interested readers can refer to these publications.

Following data are required to transform the digital values of the image into albedo values: (1) the albedo, temperature and relative humidity of the AWS (2) the coordinates of the AWS; (3) an image containing the transmittance of the atmosphere between the camera and the analysed area for each pixel of the DEM (values estimated the radiative transfer model MODTRAN (Berk et al. 2008)); (4) a map of the sky visibility for each pixel of the DEM; and (5) the angles between the camera position and the normal to the surface for each DEM pixel. The generated albedo maps underwent assessment through comparison of the camera-derived albedo with the measured albedo from the secondary AWS located on the lower glacier. The calculated and observed albedo values at this AWS showed a good agreement, with error values ranging from 5 to 9%, consistent with previous studies.

4. Results

4.1. Debris-covered surface changes

Significant surface changes were observed on the lower debris-covered glacier during the 2013–2014 period. In particular, the development of supraglacial ponds and ice cliffs is associated with the general downwasting of the glacier. A total of eight large ponds with ice cliffs were identified during this period. An example of a monitored pond and ice cliff is shown in Figure 3, where their evolution is captured thanks to the high temporal and spatial resolution of the orthoimagery. In this example, the area occupied by the pond/ice cliff doubled from $4807 \pm 158\ m^2$ to $8300 \pm 195\ m^2$ (from December 2013 to March 2014). Furthermore, the retreat of the ice cliff was observed to be on the order of tens of metres since 2013–2014, which is quite significant compared to the rest of the ice cliffs. It is important to note that most of the pond/ice cliff features are located in the lower part of the debris-covered glacier system.

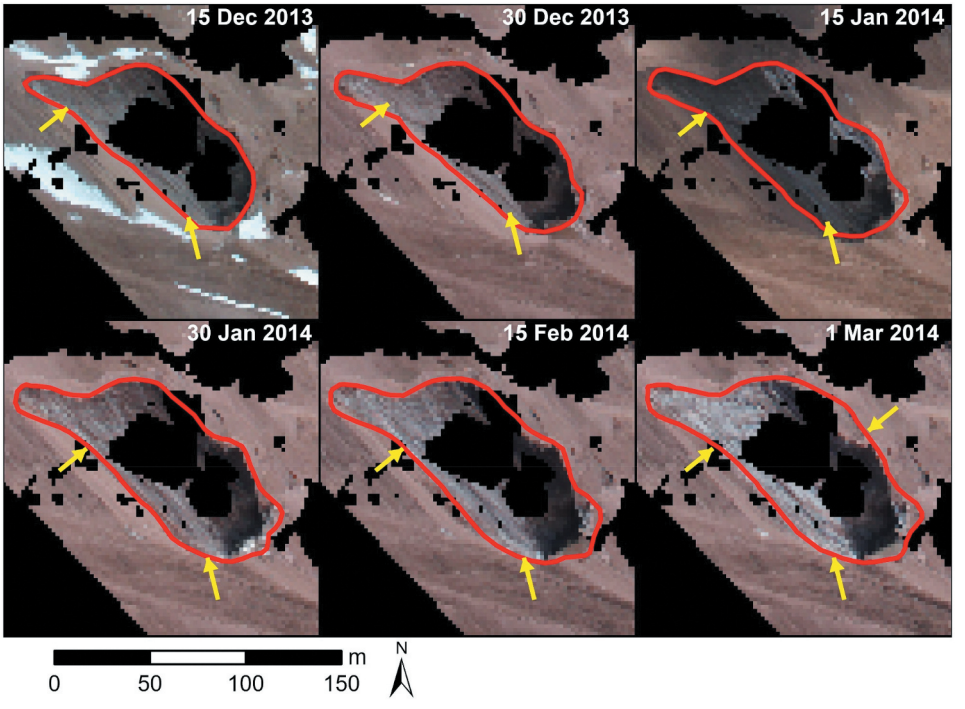

Figure 3. Evolution of an ice cliff observed (yellow arrows) on debris-covered Tapado Glacier during the summer of 2013–2014, with intervals of about 15 days. Black areas (holes) are not visible from the position of the camera.

4.2. Surface velocities

The surface flow field on the lower debris-covered glacier shows a general eastward shift, which follows the glacier's downslope movements. Between 2014 and 2015, boulder tracking and image correlation indicated average velocities of 0.2 m year^{-1} (Figure 4). Maximum velocities reached up to 0.75 m year^{-1}, located near a topographic depression (i.e., ice cliffs or ponds). Despite the obvious loss of information due to image occlusion on the orthoimage (black area in the orthoimage), the velocities of the debris-covered glacier can be estimated with an uncertainty of ±0.10 m year^{-1}. This uncertainty data was obtained from analysing apparent displacement on stable terrain in close proximity to the glacier. For a similar period, the velocities estimated for the debris-covered glacier were similar to those estimated from satellite imagery (Vivero et al. 2021). This suggests that the estimation of velocities for the debris-covered glacier using sequential time-lapse imagery is reliable and consistent with other methods. The presence of topographic depressions near areas of maximum velocities may indicate that these features play a role in accelerating ice flow.

4.3. Albedo time series

Figure 5 shows the evolution of albedo values on the Tapado site during the ablation period 2013–2014. At the beginning of the period, high albedos are evident in the upper

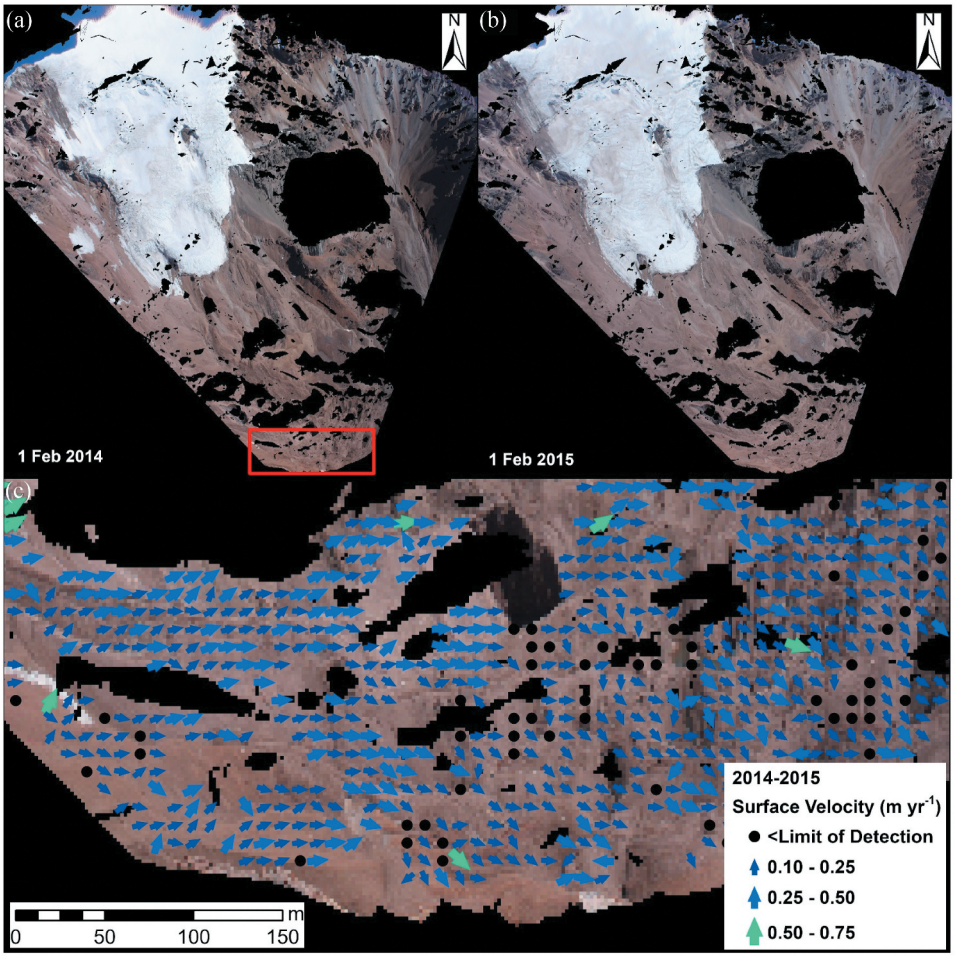

Figure 4. Surface velocities on the lower debris-covered glacier between February 2014 and February 2015. Upper right (a) and upper left (b) panels display the entire view of the orthoimages employed for feature tracking. Lower panel (c) displays the velocity flow field from the red polygon.

part of the glacier with albedo values close to 0.7. The albedo values decrease towards the front of the uncovered glacier, being even lower in the covered area of the debris-covered glacier (values close to 0.3). At the end of December, albedo values in the upper and lower part of the glacier are more uniform with values fluctuating between 0.4 and 0.2. In the debris-covered part, albedo values are generally quite low, fluctuating around 0.15. These changes in albedo values demonstrate the significant role of snow cover in the energy balance of the glacier.

The albedo changes on the glacier surface after a precipitation event are exemplified in the albedo map of December 10 (Figure 5). It can be seen here that the albedo values over the entire glacier surface have been greatly increased by the deposited fresh snow. The average albedo value on the glacier surface after the precipitation event was 0.8. However, after that date the albedo values decreased again towards values close to 0.4. This decrease in albedo is due to the fact that the snow on the

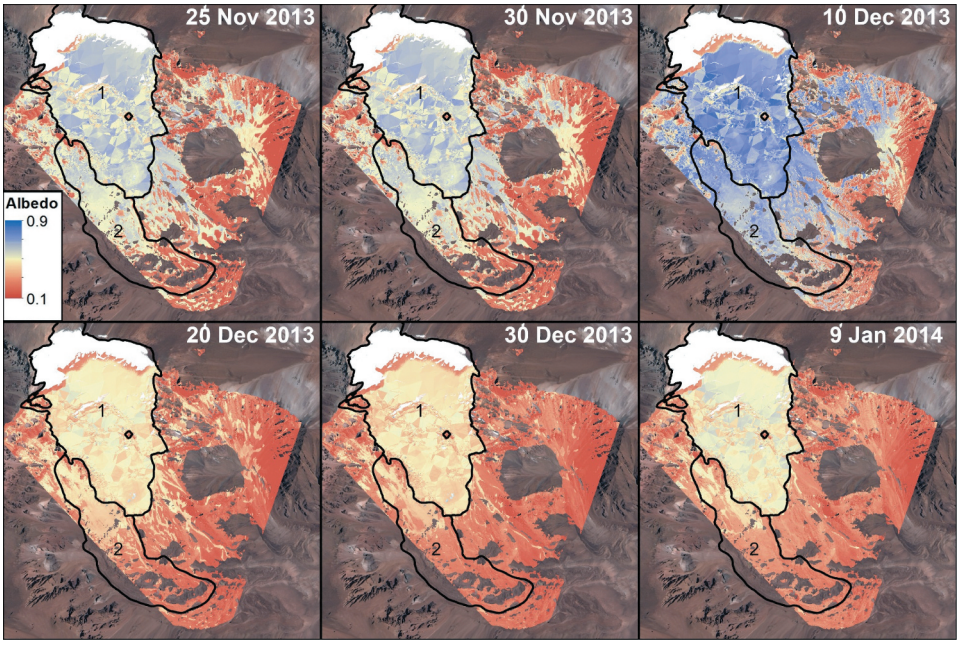

Figure 5. Examples of albedo maps during part of the ablation period 2013–2014 (November to January). Zones 1 and 2 correspond to the uncovered and debris-covered glacier, respectively. Background imagery from © CNES (2018), and Airbus DS (2018), all rights reserved.

glacier surface starts to melt, leading to more absorption of sunlight. This process is especially accelerated on the lower and sun-exposed parts of the glacier, together with the development of penitentes.

For comparison, Figure 6 illustrates the evolution of albedo during the 2014–2015 ablation period in a way that is quite different from the previous period. Here, the dramatic reduction in albedo values compared to similar periods of the previous year (Figure 5) is quite evident. In fact, this manifests a rather dry winter period with little precipitation in the region. At the beginning of the period, low albedos around 0.35 are common. As the summer progresses, the albedo values at the glacier surface decrease to 0.25, representing mostly bare ice, which highlights the high radiation absorption and the unfavourable condition for the glacier during the austral summer.

5. Discussion and conclusion

The employed methodology facilitates a straightforward and practical approach to approximating the spatial distribution of albedo across the glacier surface. Nevertheless, the presence of an uneven terrain, such as penitentes, suggests that the albedo values derived from the AWS may not accurately reflect those of a perfectly level surface. The proper integration of penitentes into energy and mass balance studies in the Central Andes (Corripio and Purves 2006), where they are prevalent at high altitudes, warrants further investigation. As a consequence, images acquired after 10 January 2014, were not processed due to a significant rise in the height of the penitentes.

Figure 6. Examples of albedo maps during part of the ablation period 2014–2015 (December to February). Zones 1 and 2 correspond to the uncovered and debris-covered glacier, respectively. One of the driest summers on record occurred during the summer of 2014–2015. Background imagery from © CNES (2018), and Airbus DS (2018), all rights reserved.

A general understanding of glacier surface behaviour can be obtained from the estimated albedo values, but their use in energy balance models needs to be considered carefully. Due to the inherent variability of albedo values, it is necessary to take more accurate measurements to obtain relevant results. It is also worthwhile to consider the temporal and spatial variability of albedo values when using them in energy balance models (Brock, Willis, and Sharp 2000). Particularly, the combination of high-resolution distributed albedos with a large coverage of satellite derived albedos can bring new insights into the understanding of glacier energy balance. For example, the role of major air pollutants emitted by mining and urban activities (transportation) in the retreat of the glacier in the Central Andes by decreasing their surface albedo (Cereceda-Balic et al. 2022) can be better monitored with in situ cameras located on different glaciers. This can also improve the implementation of Environmental Impact Assessments (EIA) that are specifically designed for glaciers and include albedo monitoring.

High-resolution georeferenced images are useful for monitoring morphometric changes in debris-covered glaciers, such as the appearance of ice cliffs and ponds. In addition, georeferenced photographs can be used to monitor surface displacements based on optical tracking of textures on debris-covered glacier surfaces. It can be used to detect potential changes in glacier dynamics by identifying zones of higher or lower velocity. Furthermore, georeferenced photographs can be used to detect new crevasses or other morphological features, as well as surface changes related to ablation and accumulation.

Potentially, the monitoring system can also be used as part of an early warning system (e.g., converting the remote camera system into a webcam). This could be used to warn of potential flooding in the event of rapid supraglacial pond formation and merging. This system can be trained on the supraglacial ponds at Tapado to monitor their development and complement this with some mitigation designs such as artificial lake control. In addition, this system can be used to track water levels and flow rates in real-time, providing valuable information to the local community during times of flooding. The data can also be used to inform local decision-making, allowing for better preparedness in the face of potential disasters.

Acknowledgments

The author thanks everyone at CEAZA involved in the project and data collection, especially Rodrigo Ponce, Cristián Campos and Shelley MacDonell. Tim Kerr also helped with the batch processing of the time-lapse images.

Disclosure statement

No potential conflict of interest was reported by the author(s).

Funding

Data were collected as part of the project 'Modelling the mass balance and water discharges from glaciers of North-Central Chile', funded by the Chilean Water Authority (Dirección General de Aguas, DGA), which is gratefully acknowledged.

ORCID

Sebastián Vivero http://orcid.org/0000-0002-1813-9575

References

Azócar, G. F., A. Brenning, and X. Bodin. 2017. "Permafrost Distribution Modelling in the Semi-Arid Chilean Andes." *The Cryosphere* 11 (2): 877–890. https://doi.org/10.5194/tc-11-877-2017.

Barandun, M., M. Huss, R. Usubaliev, E. Azisov, E. Berthier, A. Kääb, T. Bolch, and M. Hoelzle. 2018. "Multi-Decadal Mass Balance Series of Three Kyrgyz Glaciers Inferred from Modelling Constrained with Repeated Snow Line Observations." *The Cryosphere* 12 (6): 1899–1919. https://doi.org/10.5194/tc-12-1899-2018.

Berk, A., G. Anderson, P. Acharya, and E. Shettle. 2008. MODTRAN 5.2.0.0 User's Manual.

Brock, B. W., I. C. Willis, and M. J. Sharp. 2000. "Measurement and Parameterization of Albedo Variations at Haut Glacier d'Arolla, Switzerland." *Journal of Glaciology* 46 (155): 675–688. https://doi.org/10.3189/172756500781832675.

Caro, A., T. Condom, and A. Rabatel. 2021. "Climatic and Morphometric Explanatory Variables of Glacier Changes in the Andes (8–55°S): New Insights from Machine Learning Approaches." *Frontiers in Earth Science* 9 (December): 1–21. https://doi.org/10.3389/feart.2021.713011.

Casassa, G., J. L. Rodríguez, and T. Loriaux. 2014. "A New Glacier Inventory for the Southern Patagonia Icefield and Areal Changes 1986–2000." In *Global Land Ice Measurements from Space*, 639–660. Berlin Heidelberg: Springer. https://doi.org/10.1007/978-3-540-79818-7_27.

Cereceda-Balic, F., M. F. Ruggeri, V. Vidal, L. Ruiz, and J. S. Fu. 2022. "Understanding the Role of Anthropogenic Emissions in Glaciers Retreat in the Central Andes of Chile." *Environmental Research* 214 (P1): 113756. https://doi.org/10.1016/j.envres.2022.113756.

Corripio, J. G. 2004. "Snow Surface Albedo Estimation Using Terrestrial Photography." *International Journal of Remote Sensing* 25 (24): 5705–5729. https://doi.org/10.1080/01431160410001709002.

Corripio, J. G., and R. S. Purves. 2006. "Surface Energy Balance of High Altitude Glaciers in the Central Andes: The Effect of Snow Penitentes." *Climate and Hydrology in Mountain Areas* 15–27. https://doi.org/10.1002/0470858249.ch3.

DGA [Dirección General de Aguas]. 2015. Modelación Del Balance de Masa y Descarga de Agua En Glaciares Del Norte Chico y Chile Central. Santiago, Chile: Unidad de Glaciología y Nieves.

Dumont, M., Y. Arnaud, D. Six, and J. G. Corripio. 2009. "Détermination de l'albédo de surface des glaciers à partir de photographies terrestres." *La Houille Blanche* 95 (2): 102–108. https://doi.org/10.1051/lhb:2009021.

Farías-Barahona, D., Á. Ayala, C. Bravo, S. Vivero, T. Seehaus, S. Vijay, M. Schaefer, F. Buglio, G. Casassa, and M. Braun. 2020. "60 Years of Glacier Elevation and Mass Changes in the Maipo River Basin, Central Andes of Chile." *Remote Sensing* 12 (10): 1658. https://doi.org/10.3390/rs12101658.

Favier, V., M. Falvey, A. Rabatel, E. Praderio, and D. López. 2009. "Interpreting Discrepancies Between Discharge and Precipitation in High-Altitude Area of Chile's Norte Chico Region (26-32°S)." *Water Resources Research* 45 (2): 1–20. https://doi.org/10.1029/2008WR006802.

Garreaud, R. D. 2007. "Precipitation and Circulation Covariability in the Extratropics." *Journal of Climate* 20 (18): 4789–4797. https://doi.org/10.1175/JCLI4257.1.

Harrison, W. D., K. A. Echelmeyer, D. M. Cosgrove, and C. F. Raymond. 1992. "The Determination of Glacier Speed by Time-Lapse Photography Under Unfavorable Conditions." *Journal of Glaciology* 38 (129): 257–265. https://doi.org/10.3189/S002214300000366X.

Kääb, A. 2021. "Correlation Image Analysis Software (CIAS)." https://www.mn.uio.no/geo/english/research/projects/icemass/cias/.

Luhmann, T., S. Robson, S. Kyle, and J. Boehm. 2014. *Close-Range Photogrammetry and 3D Imaging. Close-Range Photogrammetry and 3D Imaging*. 2nd ed. De Gruyter. https://doi.org/10.1515/9783110607253.

Maas, H.-G., G. Casassa, D. Schneider, E. Schwalbe, and A. Wendt. 2013. "Photogrammetric Techniques for the Determination of Spatio-Temporal Velocity Fields at Glaciar San Rafael, Chile." *Photogrammetric Engineering & Remote Sensing* 79 (3): 299–306. https://doi.org/10.14358/PERS.79.3.299.

Monnier, S., C. Kinnard, A. B. Surazakov, and W. Bossy. 2014. "Geomorphology, Internal Structure, and Successive Development of a Glacier Foreland in the Semiarid Chilean Andes (Cerro Tapado, Upper Elqui Valley, 30°08′ S., 69°55′ W.)." *Geomorphology* 207 (February): 126–140. https://doi.org/10.1016/j.geomorph.2013.10.031.

Peña, M., and F. Olmedo. 2019. "Estimating Spatiotemporal Variations of Albedo in the Olivares Glaciers, Central Chile." *Revista Geográfica de Chile Terra Australis* 55 (1): 35–44. https://doi.org/10.23854/07199562.2019551.Pena35.

Robson, B. A., S. MacDonell, Á. Ayala, T. Bolch, P. R. Nielsen, and S. Vivero. 2022. "Glacier and Rock Glacier Changes Since the 1950s in the La Laguna Catchment, Chile." *The Cryosphere* 16 (2): 647–665. https://doi.org/10.5194/tc-16-647-2022.

Scapozza, C., C. Lambiel, C. Bozzini, S. Mari, and M. Conedera. 2014. "Assessing the Rock Glacier Kinematics on Three Different Timescales: A Case Study from the Southern Swiss Alps." *Earth Surface Processes and Landforms* 39 (15): 2056–2069. https://doi.org/10.1002/esp.3599.

Stehr, A., and M. Aguayo. 2017. "Snow Cover Dynamics in Andean Watersheds of Chile (32.0-39.5°S) During the Years 2000-2016." *Hydrology and Earth System Sciences* 21 (10): 5111–5126. https://doi.org/10.5194/hess-21-5111-2017.

Vivero, S., X. Bodin, D. Farías-Barahona, S. MacDonell, N. Schaffer, B. Aubrey Robson, and C. Lambiel. 2021. "Combination of Aerial, Satellite, and UAV Photogrammetry for Quantifying Rock Glacier Kinematics in the Dry Andes of Chile (30°S) Since the 1950s." *Frontiers in Remote Sensing* 2 (November): 1–17. https://doi.org/10.3389/frsen.2021.784015.

Vuille, M., and F. Keimig. 2004. "Interannual Variability of Summertime Convective Cloudiness and Precipitation in the Central Andes Derived from ISCCP-B3 Data." *Journal of Climate* 17 (17): 3334–3348. https://doi.org/10.1175/1520-0442(2004)017<3334:IVOSCC>2.0.CO;2.

Wang, A., T. Qiu, and L. Shao. 2009. "A Simple Method of Radial Distortion Correction with Centre of Distortion Estimation." *Journal of Mathematical Imaging and Vision* 35 (3): 165–172. https://doi.org/10.1007/s10851-009-0162-1.